

ARTICLE

Mechanistic Insight into the Z-E Isomerization Catalysis of Azobenzenes Mediated by Bare and Core-Shell Gold Nanoparticles

Cite this: DOI: 10.1039/x0xx00000x

Received 00th January 2012,
Accepted 00th January 2012

DOI: 10.1039/x0xx00000x

www.rsc.org/Sabrina Simoncelli^{a-c} and Pedro F. Aramendía^{*a,b}

We explored the catalytic effect of 15 nm diameter gold nanoparticles (AuNPs) upon the thermal Z-E isomerization reaction of azobenzene and nine 4 and 4-4' substituted azobenzenes (ABs). The kinetics follows a first order rate in a range of [ABs] = 5 to 50 μ M and [AuNPs] = 50 pM to 1 nM. A kinetic analysis of this compartmentalized system renders the thermal Z-E isomerization rate constant associated to each AuNP. Enhancements of 10 to 10^6 fold were measured for this rate constant in comparison to the same free ABs in solution. Experiments with selective Au facets coverage, as well as the kinetics studied in gold-silica core-shell nanoparticles (AuNP@SiO₂) of different thickness, demonstrate the surface nature of the catalysis and allow to evaluate the diffusion coefficient of azobenzene in the silica layer.

Introduction

The interaction of metallic nanoparticles (NPs) with azobenzenes has received considerable attention during the last decades in view of the changes that the photochromic transformation confers to nanoparticles properties and photocontrollable layers on metal surfaces.¹ The adsorption of switchable molecules onto NPs can modify the optical properties of the later either by local variation of the dielectric constant of the encompassing medium, due to the changes in the electronic properties of the isomers,^{2,3} or by controlling the proximity or state of aggregation of the particles upon photoisomerization.⁴⁻⁶ The isomerization efficiency of photochromic probes located in the vicinity of a NP has also attracted high interest. Metallic NPs can deactivate the electronic state of organic molecules placed near their surface through energy transfer, thus modulating the switching capability of the probe. This is a function of the photochromic – NP distance.⁷ In this approach, Whitesell et al.,⁸ reported a ~ 100-fold increase in the isomerization quantum yield of azobenzenes located at ~ 1.25 nm from the surface of a 2.5 nm diameter gold nanoparticle (AuNP) with respect to the ones located at ~ 0.54 nm. An appealing, but less studied aspect of the interaction is the analysis of the isomerization kinetic rates of azobenzenes placed near metallic NPs. In 2008, Shin et al. investigated the kinetic rates of E-Z photoconversion and Z-E thermal isomerization of an azobenzene (AB) - alkanethiol self-assembled layer of 2 nm diameter AuNP.⁹ They reported an increase between two and three times, respectively, for the isomerization rate constants compared to that of the free dye in solution. On the other hand, the group of Tamada et al., obtained identical reaction kinetics rates for 5.2 nm diameter AuNP capped with 4-hexyl-4'-(12-(dodecyldithio)dodecyloxy)azobenzene and the free AB molecules.¹⁰ Prior to the work of Yoon et al. in 2011, nobody had outlined a detailed picture of the interactions involved in the isomerization of azobenzenes near the surface of metallic NPs.⁴ In this report, by using surface enhanced Raman spectroscopy measurements, a 15

fold acceleration in the thermal Z-E isomerization kinetic rate of azobenzenes linked to AuNP aggregates was attributed to the weakening of the N-N double bond of the Z-AB isomer near the metallic surface. Further, Scaiano et al. were the first ones to report the AuNP catalysis of the thermal Z-E isomerization of unbounded 4 and 4-4'-substituted AB in suspensions of 'pseudo-naked' AuNPs.¹¹ In this case, the proposed mechanism involves the formation of an azobenzene radical cation intermediate through electron transfer from the probe to the gold surface. In this work, average rates were measured in this AuNP suspension in water. In this contribution, we have thus examined the kinetics of the thermal Z-E isomerization for a family of 4 or 4-4' substituted azobenzenes in AuNPs suspensions with the aim at answering the following questions: Which is the magnitude of the catalytic effect of the AuNPs? Can we obtain the Z-E thermal isomerization rate of azobenzenes over the AuNPs? Which is the role of the metallic surface? Is it necessary for the photochromic compound to be in direct contact with the metallic surface or does the NP influence on the catalysis extend in volume due to the high polarizability of the NP plasmonic interaction? Which is the influence of the substituents in the isomerization catalysis? Which is the role of the pH of the medium?

Results

Figure 1 shows transmission electron microscopy (TEM) micrographs and histograms of the size distribution of the AuNP and the silica coated AuNP (AuNP@SiO₂) used in this work.

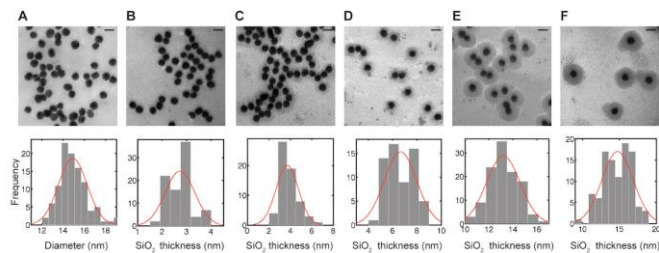


Figure 1. TEM micrographs (upper panel) and size histograms (lower panel) of (A) AuNPs of 15 ± 1 nm diameter and AuNP@SiO₂ with increasing SiO₂ shell thickness (B) 2.7 ± 0.6 nm; (C) 4 ± 1 nm; (D) 7 ± 1 nm; (E) 13 ± 1 nm and (F) 15 ± 2 nm. Scale bars: 20 nm in all cases. Histograms were constructed with sample set size $n > 50$.

Catalyzed Z-E thermal isomerization by AuNPs was observed for AB (Figure 2) and the following nine 4 or 4'-substituted azobenzenes: DM-AB; DC-AB; DEO-AB; MO-AB; NO₂-AB; NO₂-MOAB; NO₂-DAB; DABCYL and NO₂-HAB (Figures 3 and S3). Figure 2, 3, and S3 show the temporal spectral evolution of azobenzenes in a AuNP suspension. The spectral information of the AuNPs/azobenzene systems correspond to the characteristic spectral changes of the Z \rightarrow E isomerization reaction for the free dye in solution, for example, for AB, increase of the $\pi - \pi^*$ band ($\lambda_{\text{max}} \sim 320$ nm) and decrease of the $n - \pi^*$ ($\lambda_{\text{max}} \sim 450$ nm) band (Figure 2-A) and they are invariant in the presence of AuNPs.^{12,13}

The small scattering by the AuNP did not affect the measurements since the kinetic data were derived from differential absorption data (see Figures 2 and 3).

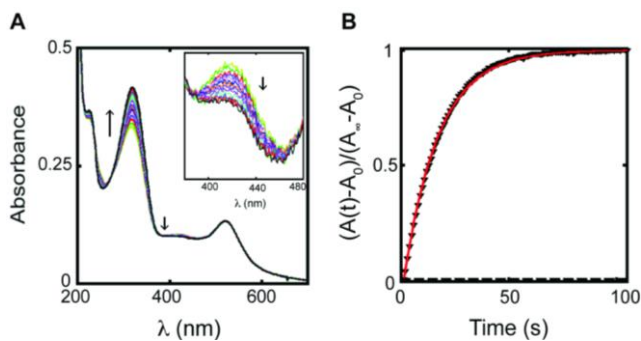


Figure 2. (A) UV-Vis temporal evolution of a 15 μ M AB aqueous solution with 300 pM AuNPs suspension (diameter = 15 ± 1 nm) measured after the UV photolysis flash. The inset enlarges the spectral region of the $n - \pi^*$ band. The band with maximum around 520 nm represents the AuNPs extinction. (B) Growth of the E isomer concentration measured at 320 nm (black triangles). The red line is the monoexponential fit to the experimental data. The dashed black line near the abscissa axis represents the temporal evolution of the E isomer in the absence of AuNPs in this time interval.

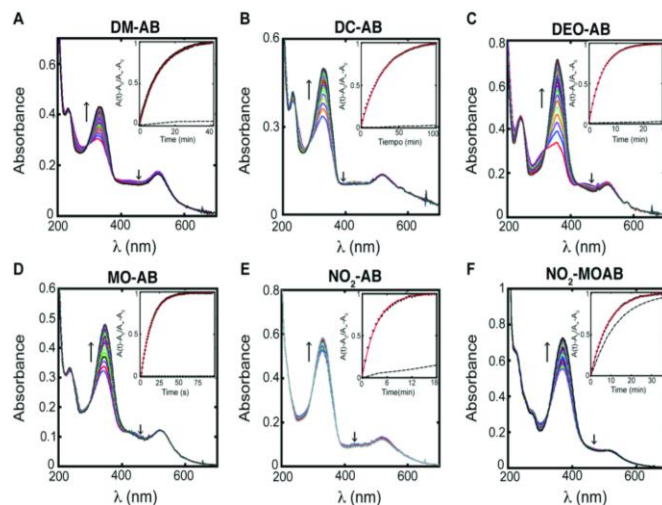


Figure 3. UV-Vis temporal evolution of a 300 pM or 400 pM AuNPs suspension (diameter = 15 ± 1 nm) and 10 μ M E (A) DM-AB; (B) DC-AB; (C) DEO-AB; (D) MO-AB; (E) NO₂-AB and (F) NO₂-MOAB solution after the UV photolysis flash. The inset corresponds to the growth of the E isomer concentration measured at (A) 330 nm; (B) 330 nm; (C) 360 nm; (D) 345 nm; (E) 330 nm; and (F) 370 nm. The red lines represent the monoexponential fit to the experimental data. The dashed black line corresponds to the temporal evolution of the E isomer in the absence of AuNPs in the same time interval.

Figure 2-B, Figure S3, and the insets in Figure 3 display the time evolution of the build up of the E isomer in AuNPs suspensions. The kinetics follows a first order rate with very good approximation in all cases, and in a range of $[AB] = 5$ to 50 μ M and $[AuNPs] = 50$ pM to 1 nM. This points to the fact that the Z-E isomerization is rate determining compared to other dynamic events. Specifically, the addition of 0.3 to 0.4 nM AuNPs of 15 nm diameter to 10 μ M azobenzene solutions resulted in accelerated Z-E isomerization. The high activity of AuNPs catalysis gives rise to a 10^4 fold increase in the global first order isomerization rate constant, k_{obs} , of AB and MO-AB in suspensions of AuNPs in water. On the other hand, for the systems of AuNPs and symmetrically substituted azobenzenes (DM-AB; DC-AB; DEO-AB) in mixtures of acetonitrile (ACN):water (5:1) the isomerization reaction is accelerated ~ 100 times with respect to the free dye in solution. For NO₂-AB and NO₂-MOAB (also in 5:1 ACN:water) the catalytic acceleration of the Z-E isomerization is much lower: a factor of 30 and 2, respectively. Regarding NO₂-DAB and DABCYL a 10^3 times increase is observed for the thermal isomerization rate, while a 50-fold increase is detected for NO₂-HAB.

The addition of AuNPs to the reaction medium provokes a decrease in the pH. Further, it is well known that acidic pH highly increases the Z-E thermal isomerization rate in azobenzenes.¹⁴⁻¹⁷ Therefore, control experiments were performed for azobenzenes solutions at the same pH of the AuNPs suspensions but in the absence of AuNPs. The isomerization kinetics for AB; DM-AB; DC-AB; DEO-AB; MO-AB; NO₂-AB and NO₂-MOAB, in such control experiments, was identical to the ones observed for the corresponding azobenzenes in solution in the absence of acid and AuNPs (see Figure S4). On the other hand, for NO₂-DAB; DABCYL and NO₂-HAB the isomerization rate constant for samples with the same pH are identical, regardless of the presence or absence of AuNPs (see Figure S5). Thus, a potential AuNPs catalytic action upon the thermal Z-E isomerization reaction for these three last mentioned azobenzenes is masked by the changes in acidity that AuNPs addition causes to the solution.

Figure 4-A and 4-B illustrate the dependence of k_{obs} with [AuNP] and [AB] concentration, respectively.

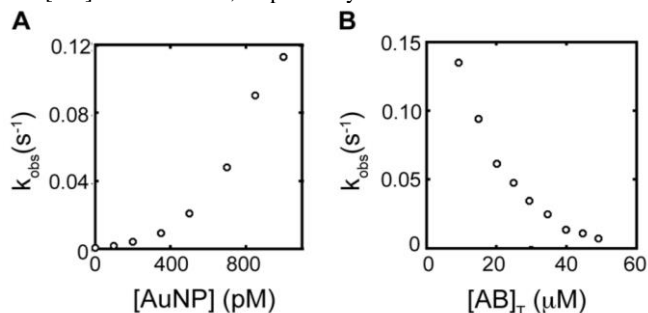


Figure 4. Dependence of the Z-E thermal isomerization first order rate constant for an aqueous solution (A) on the AuNP concentration (50 μM AB), and (B) on the AB concentration (300 pM AuNPs). The diameter of the AuNPs is 15 ± 1 nm.

The trends can be interpreted considering a reaction scenery where Z isomers decay to the stable E form either in the continuous solution phase or under the influence of the dispersed AuNPs that accelerate the reaction rate. Thus, the increase of k_{obs} with AuNPs concentration relates to an increase in the relative amount of Z molecules influenced by AuNPs. On the other hand, increase of AB in the medium decreases the molar fraction of AB molecules associated with AuNPs, which in turn is manifested as a decreased reaction rate constant. From these experiments it stands out that the magnitude of the observed Z \rightarrow E first-order kinetic rate constant only depends on the relative AB - AuNP concentration (see Figures 5 and S7).

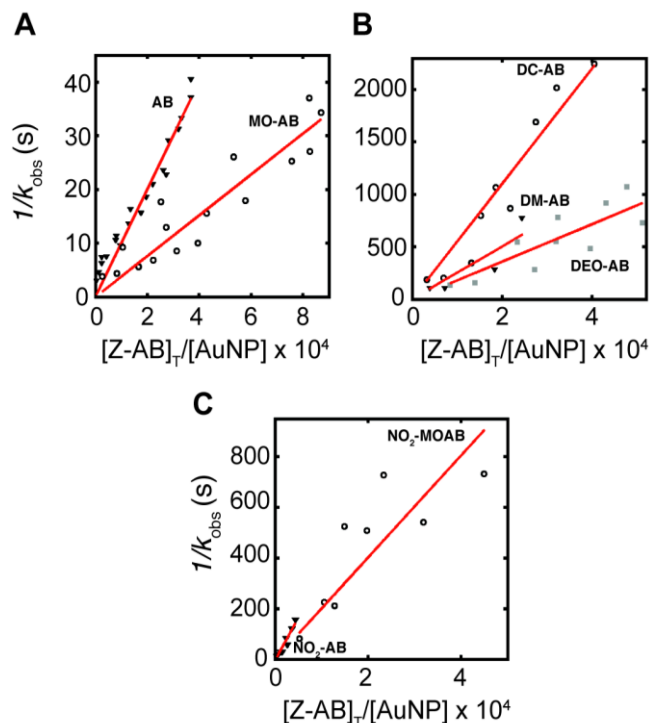


Figure 5. Inverse of the thermal Z-E isomerization reaction rate constant as a function of the $[\text{Z-AB}]_{\text{T}}/[\text{AuNP}]$ for (A) aqueous and (B-C) ACN:water (5:1) solutions of different azobenzenes/AuNPs systems. The red line represents the best linear fit (see eq. 2).

The catalytic surface of a metal is heterogeneous by nature.¹⁸ One of the main objectives in catalysis is to determine the number of

catalytically different sites and the contribution of each of them in the global reaction. In this regard, a common approach is to use target-blocking agents to determine the changes of reactivity.^{19,20} Poli(vinyl pyrrolidone) (PVP) selectively binds to gold and silver {100} facets.²¹ On the other hand, sodium citrate binds stronger to {111} compared to {100} facets. Therefore, we decided to functionalize the citrate stabilized 15 nm AuNPs (bare AuNPs) with PVP, poisoning the catalytic activity of the {100} facets of the AuNPs. Figure 6 shows k_{obs} as a function of the relative concentration of Z-AB and AuNPs for experiments with (empty circles) and without (black triangles) PVP functionalization.

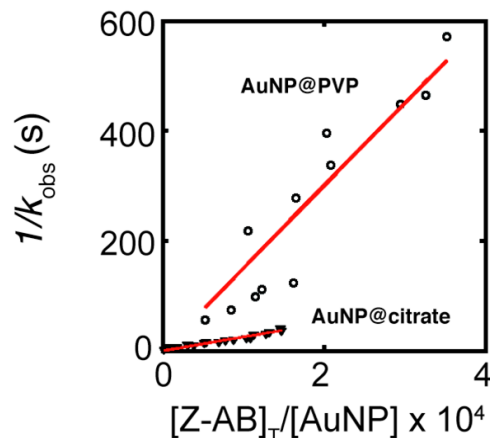


Figure 6. Inverse of the thermal Z-E isomerization reaction rate constant as a function of the $[\text{Z-AB}]_{\text{T}}/[\text{AuNP}]$ for aqueous solution of azobenzenes and citrate stabilized (black triangles) or PVP-functionalized AuNPs (empty circles). The red line represents the best linear fit (see eq. 2).

Interestingly, PVP-functionalized AuNPs samples are much less efficient for the catalyzed thermal Z-E isomerization reaction than the bare-AuNPs. This can be explained as a decrease in the number of AB binding sites per AuNP in the presence of PVP to the more reactive {100} facets.

Time dependence evolution of the catalytic growth of E-AB by PVP covered (blue circles) and silica-coated (green triangles and red squares) AuNPs is presented in Figure 7.

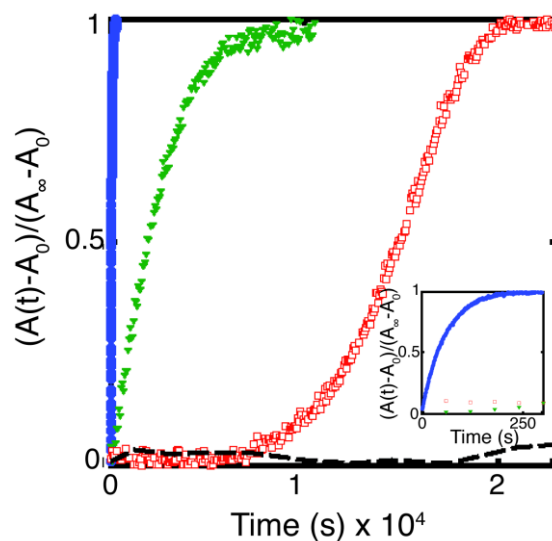


Figure 7. Growth of the E-AB isomer concentration measured at 320 nm for ethanolic solutions of 8 μM AB in suspension of: 2 nM, 15 ± 1 nm diameter, AuNPs.

PVP functionalized AuNPs (blue circles); 1 nM AuNPs@SiO₂ with 4 ± 1 nm (green triangles); 15 ± 2 nm (red squares) silica shell thickness; and 2 nM 71 ± 8 diameter silica nanoparticles (black dashed line) immediately after the addition of NPs and the UV photolysing flash. The inset corresponds to a time range expansion for the reaction catalyzed by PVP covered gold nanoparticles.

AuNPs@SiO₂ synthesis requires transferring AuNPs from water to ethanol solutions using PVP as the coupling agent. Thus, bare AuNPs were functionalized with PVP and dispersed in ethanolic media for strict data comparison. Adsorption effects over SiO₂ were discarded in a control experiment that gave equal isomerization rate constants for free AB in solution and for AB in suspensions of silica NPs (without Au core) (dashed line, Figure 7). The isomerization rate constant for PVP functionalized AuNPs is ~ 35 fold higher than the corresponding for 4 ± 1 nm thicknesses AuNPs@SiO₂. Further, the sigmoidal temporal dependence for the E-AB growth observed for 15 ± 2 nm silica shell thicknesses core-shell NPs (red squares, Figure 7) points to a diffusion controlled process. Specifically, immediately after NPs addition, there is an initial delay time that allows Z-AB molecules to diffuse sufficiently close to the Au core to exhibit Z-E catalyzed reaction. The exponential increase of the absorbance of the E isomer is delayed as the reaction proceeds to complete conversion to this isomer.

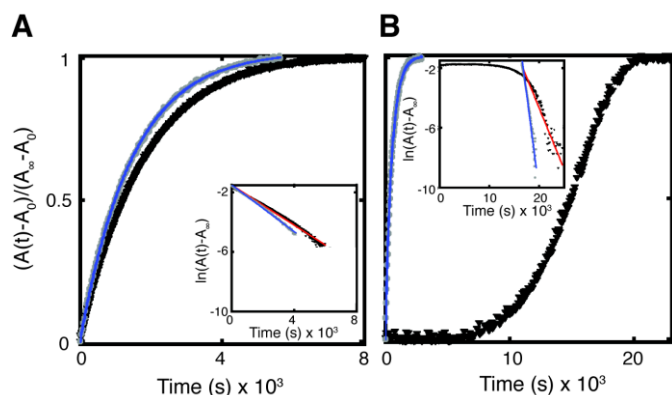


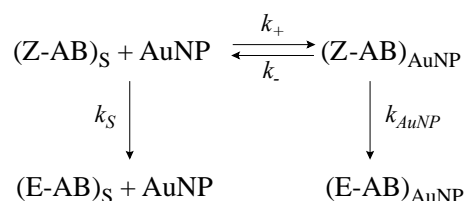
Figure 8. Growth of the E-AB isomer concentration measured at 320 nm for ethanolic solutions of 8 μM AB in suspension of AuNPs@SiO₂: (A) 2.7 ± 0.6 nm ([AuNP] = 0.8 nM) and (B) 15 ± 2 nm ([AuNP] = 1.0 nM) silica shell thickness immediately after (black triangles) or after 12 hs (grey circles) NPs addition. The blue lines are the monoexponential fits to the data. The insets correspond to the logarithmic representation of the absorbance growth. The data recorded immediately after NPs addition were temporally delayed for a better comparison. The blue and red lines correspond to the best linear fits.

Evaluation of the diffusion regime observed in the different silica shell thicknesses of AuNPs@SiO₂ was performed by comparing the temporal build up of the E concentration isomer immediately after NPs addition (Figure 8, black triangles) and after leaving the AB/AuNPs@SiO₂ solution incubate in the dark overnight (Figure 8, grey circles). The thinner silica shell AuNPs@SiO₂ tested, 2.7 ± 0.6 nm, displays almost the same temporal dependence for the E isomer growth, independently of the mixing time in the dark before photolysis (Figure 8-A). Therefore, AB reaches stationary diffusion regime in the silica layer during the Z isomer decay for this thickness. On the other hand, for NPs with the thickest silica shells, faster Z-E conversion is detected after allowing azobenzenes molecules to diffuse inside the silica layer overnight (Figure 8-B and Figure S8). This indicates non-stationary diffusion regime for AB molecules in silica shells thicker than 2.7 ± 0.6 nm immediately after NPs addition. Insets of Figure 8 show the log data representation for the exponential growth phase of the kinetic traces. Parallel curves point to stationary state diffusion regime for AB in the silica layer.

Distinctively, while for 2.7 ± 0.6 nm silica shell thickness parallelism of both plots is observed, the thicker the silica layer, the higher is the ratio of slopes between the incubated and the as prepared samples. This ratio is 2 for 4 ± 1 nm thickness and 3 for 7 ± 1 nm, 13 ± 1 nm, and 15 ± 2 nm silica layers.

Discussion

The kinetics and mechanism of the catalyzed thermal back isomerization of azobenzenes in AuNPs suspensions is analyzed by studying the dependence of k_{obs} as a function of the relative AB - AuNP concentration (see Figures S7 and 5).



Scheme 1. Mechanism for the microheterogeneous dark Z-E isomerization catalyzed by AuNPs.

To interpret the physicochemical meaning of the observed first order rate constant, we propose a compartmentalized reaction scenery (see Scheme 1) where the Z and E isomers distribute in two phases, the dispersed phase (formed by the sum of the volume of influence of all the AuNPs), and the continuous (solvent) phase. Assuming rapid equilibration for the reactant exchange steps between compartments compared to the reactive steps, (i.e. $k_+[Z-AB]_S$; $k_- \gg k_S$; k_{AuNP}), and neglecting reactant exchange by direct AuNP interactions, the first order reaction rate constant can be expressed as a weighted average of the first order isomerization rate constants in solution, k_S , and in the vicinity of AuNPs, k_{AuNP} (uncatalyzed and catalyzed reaction pathways, respectively). The weighting factors are the mole fractions of Z-AB molecules associated to each phase. Further, expressing the concentration of the Z isomer in the disperse phase as a function of the average number of Z molecules associated to each single AuNP, $\langle n \rangle$, the following expression for k_{obs} can be obtained (see S6),

$$k_{obs} = k_S + \frac{\langle n \rangle [AuNP]}{[Z-AB]_T} \cdot (k_{AuNP} - k_S) \quad (\text{eq. 1})$$

where $[Z-AB]_T$ is the total concentration of Z-AB isomer obtained immediately after the photolysing flash. It is evaluated from the difference absorption spectrum.

For all the studied azobenzenes and for all the combinations of $[AuNP]/[AB]$ tested it holds that $k_{obs} \gg k_S$, accordingly $k_{AuNP} \gg k_S$, and therefore, eq. 1 can be simplified to eq. 2,

$$k_{obs} = \frac{\langle n \rangle [AuNP]}{[Z-AB]_T} \cdot k_{AuNP} \quad (\text{eq. 2})$$

Figure 5 displays the inverse of k_{obs} as a function of $[Z-AB]_T/[AuNP]$ for different azobenzenes-AuNPs systems. As expected, increase of k_{obs} as a function of $[AuNP]/[Z-AB]_T$ is related to a higher proportion of Z-AB molecules associated to the disperse phase. The linear relationship observed in Figure 5 suggests that $\langle n \rangle$ is a constant value in the concentration range tested.

The experiments with PVP blocking the {100} facets give the hint to the predominant surface character of the catalysis and points to these planes as the more catalytically active ones. The experiments

performed with AuNPs@SiO₂ suspensions allowed the further elucidation of the spatial catalytic extension of the AuNPs. Particularly, it was possible to determine whether the isomerization catalysis was active at nm distance from the AuNP surface or if it only takes place upon direct contact with the metallic surface. The distinct catalytic behavior for even the thinner silica shell AuNPs@SiO₂ with respect to the bare NPs as well as the competitive experiments with PVP, enlightens the surface catalytic nature of the AuNPs on the Z-E isomerization in azobenzenes. On the other hand, the constant average number of Z molecules associate to each single AuNP evidenced in the kinetic experiment can be considered as the maximum number of available adsorption sites in the surface of each AuNP, n_{max} . This later parameter can be estimated using different assumptions. In this work, it was approximated as 10³ binding sites for a 15 nm diameter AuNP and considered independent of the derived structure of the azobenzene (see S7 for detailed calculation).

The acceleration of the reaction rate constant measured on Au {100} facets is in line with the reported reduction of the activation energy by a factor of four for the thermal Z-E isomerization of adsorbed tetra-*tert*-butyl-azobenzene on Au {111} compared to the free molecule in the liquid phase.²² In another work, the authors find a change in the lifetime of 3-(4-(4-hexyl-phenylazo)-phenoxy)-propane-1-thiol from more than 35 h in dichloromethane solution to ca 60 s in self assembled mixed monolayer with n-butanethiol on Au {111}.²³

Table 1 reports the values of k_{AuNP} calculated from the best linear fit of the experimental data of Figure 5. The enhancement factor in k_{AuNP} for AB and MO-AB in aqueous suspensions of AuNPs is in the order of 10⁵. On the other hand, DM-AB, DC-AB and DEO-AB experiment a 10³ fold acceleration in suspensions of ACN:water (5:1). Further, NO₂ substituted azobenzenes only show a 10² or 10¹ AuNP catalytic factor in this same solvent mixture.

Table 1. Parameters of the best linear fit of the inverse of equation 2 for the experimental data of Figure 5.

Azobenzene	$n_{max} k_{NP} (s^{-1})$	$k_{NP} (s^{-1})^*$	$k_S (s^{-1})$	k_{NP} / k_S
AB	1×10^3	1×10^0	1×10^{-6}	1×10^6
DM-AB	4×10^1	4×10^{-2}	7×10^{-6}	6×10^3
DC-AB	2×10^1	2×10^{-2}	6×10^{-6}	4×10^3
DEO-AB	6×10^1	6×10^{-2}	3×10^{-5}	2×10^3
MO-AB	3×10^3	3×10^0	6×10^{-6}	5×10^5
NO ₂ -AB	3×10^1	3×10^{-2}	1×10^{-4}	2×10^2
NO ₂ -MOAB	5×10^1	5×10^{-2}	1×10^{-3}	4×10^1

* Obtained considering in all cases $n_{max} = 10^3$ (see S7).

The acceleration of the reaction rate induced by AuNPs is related to the weakening of the azo double bond character on the surface of the gold nanoparticle.⁴ Azobenzenes carrying an electronegative group present intrinsically weaker -N-N- double bond character and therefore the expected AuNP catalytic effect should be poorer. However, if we only consider the electronegativity factor of the azobenzene substituents, we cannot explain the acceleration observed for the MO-AB Z-E thermal isomerization relative to the symmetrically substituted azobenzenes such as, DM-AB, or DC-AB. To approach an explanation of this fact, we should take into account that ACN reversibly adsorbs on the gold surface with a binding energy of 46 kJ/mol onto the Au(100) facets,²⁴ thus competing with the azobenzenes molecules for the adsorption sites ($E_{ad} \sim 160$ kJ/mol for Au(111)).²⁵ Therefore, decrease in the global isomerization

reaction rate constant for systems measured in ACN:water (5:1) with respect to the ones measured in water can be attributed to a decrease in the value of n_{max} . Further, the NO₂ groups can also be reversibly adsorbed on the gold surface ($E_{ad} \sim 58.6$ kJ/mol for Au(111))²⁶ and therefore compete with the azo moiety for the surface binding sites, without the same effect in the reactive rate.

Finally, we can use the kinetic curves in AuNPs@SiO₂ to estimate the diffusion coefficient of AB in silica, D_{AB-SiO_2} , by solving Fick's equation for steady state diffusion in a spherical geometry (see S8). Equation 3 holds for the D_{AB-SiO_2} as a function of the diffusion kinetic rate constant, k_{diff} , the AuNPs radius, r_{NP} , the thickness of the silica shell, h_{SiO_2} , and [AuNPs].

$$D_{AB-SiO_2} = \frac{k_{diff}}{4\pi \cdot [AuNP] \cdot N_A} \cdot \frac{h_{SiO_2}}{r_{NP}(r_{NP} + h_{SiO_2})} \quad (\text{eq. 3})$$

Table 2. Diffusion rate constant, k_{diff} , and diffusion coefficient, D_{AB-SiO_2} , for AB molecules in silica as a function of silica shell thickness, h_{SiO_2} . k_{diff} was determined with the best monoexponential fit of the data of Figure 7 and Figure S8 (grey circles). The D_{AB-SiO_2} was calculated using eq. 3.

h_{SiO_2} (nm)	$k_{diff} (10^3 s^{-1})$	$D_{AB-SiO_2} (10^{-11} cm^2/s)$
2.7 ± 0.6 nm	0.68	1.1 ± 0.5
4 ± 1 nm	0.82	1.6 ± 0.7
7 ± 1 nm	1.6	5 ± 2
13 ± 1 nm	1.8	11 ± 4
15 ± 2 nm	1.9	8 ± 3

Table 2 summarizes k_{diff} and D_{AB-SiO_2} for the different silica shell thickness. The small diffusion coefficient for AB in silica ($\sim 10^{-10}$ - 10^{-11} cm²/s) in comparison to free diffusion of AB in water ($\sim 10^{-6}$ cm²/s)²⁷ relates to a tortuous pathway for diffusing molecules inside the disordered and microporous silica shell (estimated porous size of ~ 15 Å).²⁸ Further, the hydrophilic silica pores (active hydroxyl groups) may promote the adsorption of molecules in the silica pores (chemical traps) precluding the arrival of Z-AB molecules to the gold surface. Regarding to the higher D_{AB-SiO_2} values for thicker silica shells this can be understood as a more compact silica matrix for the proximal layers compared to the more expanded outer part.

Conclusions

Z-E thermal isomerization reaction of 4 or 4-4' substituted azobenzenes is highly accelerated in sub nM 15 ± 1 nm diameter AuNPs suspensions. Microheterogeneous kinetic analysis was found useful to describe the combined process of the thermal Z isomer decay in the continuous solution phase and under the catalytic influence of the dispersed AuNPs. With this approach it was possible to determine the first order isomerization rate constants in the vicinity of AuNPs. The magnitude of the acceleration is not only determined by the nature of the substituents but also by the solvent and surfactants present in the reaction medium. The maximum acceleration factor detected, of 10⁶ times, was for AB in aqueous solution and in the absence of external surfactants. The competitive adsorption of acetonitrile, polyvinylpyrrolidone (PVP) and NO₂ groups in the azo moiety binding sites of the gold surface masks the AuNPs catalytic effect. Selective blocking experiments with PVP suggested that the {100} crystalline facets are particularly active for the

catalysis. Experiments performed with core shell AuNP with different silica spacer around the gold surface reveal the exclusive surface nature of the AuNP mediated catalysis. Further, it was possible to determine the diffusion coefficient of AB in silica layers as $D_{AB-SiO_2} \sim 10^{-10} - 10^{-11} \text{ cm}^2/\text{s}$.

Experimental

Chemicals.

All reagents were used as received unless specified otherwise: HAuCl₄·3H₂O (≥ 99.9%, Aldrich); trisodium citrate dihydrate (≥ 99%, Aldrich); 2-hydroxy-4'-(2-hydroxyethoxy)-2-methylpropionophenone (Irgacure 2959) (98%, Aldrich); tetraethyl orthosilicate (≥ 98.0%, Fluka) (TEOS); (3-aminopropyl)triethoxysilane (≥ 98%, Sigma Aldrich); polyvinylpyrrolidone (PVP10) (average molecular weight 10,000 g/mol, Sigma Aldrich); acetonitrile (HPLC grade, Sintorgan); Azobenzene (98%, Sigma Aldrich) (AB); 4-methoxyazobenzene (≥ 99.0%, Aldrich) (MO-AB); 4-nitroazobenzene (90%, Aldrich) (NO₂-AB); 4,4'-dimethylazobenzene (Aldrich^{CPR}) (DM-AB); 4,4'-dichloroazobenzene (Aldrich^{CPR}) (DC-AB); 4,4'-diethoxyazobenzene (97%; ALFA AESAR) (DEO-AB); 4-nitro-4'-methoxyazobenzene (NO₂-MOAB); 4-nitro-4'-dimethylaminoazobenzene (≥ 98.0%, TCI) (NO₂-DAB); 4-(4'-nitrophenylazo)phenol (≥ 97.0%, TCI) (NO₂-HAB); 4-[4-(Dimethylamino)phenylazo]benzoic acid N-succinimidyl ester (Sigma Aldrich) (DABCYL). The following reagents were all of analytical grade: hydrochloric acid, ammonia, ethanol, sodium hydroxide.

Nanoparticle synthesis.

Au nanoparticles with an average radius of $15 \pm 1 \text{ nm}$ (see Figure 1) were prepared following the Turkevich protocol.²⁹ 'Semi-naked' gold nanoparticles were photochemically synthesized as described elsewhere³⁰ obtaining nanoparticles with a mean radius of $10 \pm 2 \text{ nm}$ (see Figure S1). Au-SiO₂ core-shell nanoparticles (AuNP@SiO₂) of 2.7 ± 0.6 ; 4 ± 1 ; 7 ± 1 ; 13 ± 1 , and $15 \pm 2 \text{ nm}$ silica shell thicknesses (see Figure 1-B to F) were synthesized following van Blaaderen procedure.³¹ Briefly, PVP10 was used as a coupling agent to transfer the colloids from water to a 4.2% v/v ammonia-ethanol medium. Silica deposition over the gold core was performed by quickly adding TEOS under vigorous stirring. The solution was kept under stirring at room temperature for 12 hs. The silica-coated nanoparticles were purified by 3 cycles of redispersion in ethanol and centrifugation at 12,000 RCF. The final concentration of the nanoparticle solution was determined by gold quantification of the nanoparticle suspension with graphite furnace atomic absorption spectrometry. Silica nanoparticles (mean radius = $71 \pm 8 \text{ nm}$, see Figure S2) employed as control samples were prepared following a standard Stöber protocol.³²

Spectroscopy.

UV-VIS spectra were measured on a Hewlett Packard 8452A, on a Shimadzu UV3101PC (Shimadzu Corporation, Kyoto, Japan), or on a Cary 50 UV-Vis (Agilent Technologies, Santa Clara, USA). Laser flash photolysis experiments were carried out using a Surelite-II OPO Plus (pump with a Nd-YAG 355 nm) (Continuum, Santa Clara, USA) as the excitation source. Data was recorded with a LFP 111 laser-flash photolysis system (Luzchem Inc., Ottawa, Canada).

System characterization.

Nanoparticles mean radius and silica shell thickness were measured by either transmission electron microscopy (TEM) in a Philips EM 301 apparatus or by scanning electron microscopy (SEM) in a JEOL JSM-7500F equipment.

Sample Preparation. Typical experiments were performed in 1 cm x 1 cm quartz cuvettes combining 50 to 500 μL of AuNPs or

AuNP@SiO₂ with water or ethanol or mixtures of acetonitrile-water until a final volume of 3 mL was reached. Kinetic experiments were performed after gradual addition of 5 to 45 μL of 5 mM or 1 mM ACN solutions of the corresponding AB to the previous mentioned NPs suspension. All azobenzenes/AuNPs suspensions except for AB and MO-AB were prepared in 5:1 ACN:water mixtures. E-Z photochemical conversion was performed with either a commercial photographic xenon flash lamp or with the corresponding excitation wavelength of the OPO laser. For the pH dependence experiments solutions of HCl or NaOH were also used.

Acknowledgements

PFA is research staff and SS is a research fellow from CONICET. The work was performed under support from CONICET (PIP 11220100100397) and UBA (Grant Number: 20020100100234). SS acknowledges ELAP (Emerging Leaders in the Americas Program) for the DFAIT fellowship to support her visit to Canada. We thank Prof. Juan C. Scaiano (University of Ottawa) for helpful suggestions and for providing the facility to perform the laser flash photolysis experiments and to synthesize the 'semi-naked' gold nanoparticles.

Notes and references

^a Centro de Investigaciones en Bionanociencias "Elizabeth Jares-Erijman" (CIBION-CONICET) Godoy Cruz 2390, 1425 Buenos Aires, Argentina.

^b Departamento de Química Inorgánica, Analítica y Química Física, Facultad de Ciencias Exactas y Naturales, Universidad de Buenos Aires, Pabellón 2. Ciudad Universitaria. 1428 Buenos Aires, Argentina.

^c Instituto de Química Física de Materiales, Ambiente y Energía, (INQUIMAE-CONICET). Pabellón 2. Ciudad Universitaria. 1428 Buenos Aires, Argentina.

Electronic Supplementary Information (ESI) available: .Gold nanoparticle characterization, kinetics traces for NO₂-DAB; DABCYL and NO₂-HAB thermal Z-E isomerization, pH control experiments, global kinetic rate influence on the relative ABs - AuNPs concentration, kinetic traces for the Z-E isomerization of AB in suspensions of different thickness of AuNPs@SiO₂, determination of the AuNP associated first order thermal isomerization rate constant, derivation of the diffusion equation. See DOI: 10.1039/b000000x/

- 1 R. Klajn, J. F. Stoddart and B. a Grzybowski, *Chem. Soc. Rev.*, 2010, **39**, 2203–37.
- 2 Y. B. Zheng, Y.-W. Yang, L. Jensen, L. Fang, B. K. Juluri, A. H. Flood, P. S. Weiss, J. F. Stoddart and T. J. Huang, *Nano Lett.*, 2009, **9**, 819–825.
- 3 S. J. van der Molen, J. Liao, T. Kudernac, J. S. Agustsson, L. Bernard, M. Calame, B. J. van Wees, B. L. Feringa and C. Schönenberger, *Nano Lett.*, 2008, **9**, 76–80.
- 4 J. H. Yoon and S. Yoon, *Phys. Chem. Chem. Phys.*, 2011, **13**, 12900–12905.
- 5 R. Klajn, K. J. M. Bishop and B. a Grzybowski, *Proc. Natl. Acad. Sci. U. S. A.*, 2007, **104**, 10305–9.
- 6 D. S. Sidhaye, S. Kashyap, M. Sastry, S. Hotha and B. L. V Prasad, *Langmuir*, 2005, **21**, 7979–7984.
- 7 E. Dulkeith, A. C. Morteani, T. Niedereichholz, T. A. Klar, J. Feldmann, S. A. Levi, F. C. J. M. van Veggel, D. N. Reinhoudt, M. Möller and D. I. Gittins, *Phys. Rev. Lett.*, 2002, **89**, 203002.
- 8 J. Zhang, J. K. Whitesell and M. A. Fox, *Chem. Mater.*, 2001, **13**, 2323–2331.
- 9 K. Shin and E. J. Shin, *Bull. Korean Chem. Soc.*, 2008, **29**, 1259–1262.
- 10 A. Manna, P.-L. Chen, H. Akiyama, T.-X. Wei, K. Tamada and W. Knoll, *Chem. Mater.*, 2003, **15**, 20–28.
- 11 G. L. Hallett-Tapley, C. D'Alfonso, N. L. Pacioni, C. D. McTiernan, M. González-Béjar, O. Lanzalunga, E. I. Alarcon and J. C. Scaiano, *Chem. Commun.*, 2013, **49**, 10073–5.

- 12 N. Nishimura, T. Sueyoshi, H. Yamanaka, E. Imai, S. Yamamoto and S. Hasegawa, *Bull. Chem. Soc. Jpn.*, 1976, **49**, 1381–1387.
- 13 P. P. Birnbaum, J. H. Linford and D. W. G. Style, *Trans. Faraday Soc.*, 1953, **49**, 735–744.
- 14 G. S. Hartley, *J. Chem. Soc.*, 1938, **113**, 633–642.
- 15 N. J. Dunn, W. H. Humphries, A. R. Offenbacher, T. L. King and J. a Gray, *J. Phys. Chem. A*, 2009, **113**, 13144–51.
- 16 A. M. Sanchez and R. H. Rossi, *J. Org. Chem.*, 1995, **60**, 2974–2976.
- 17 S. Ciccone and J. Halpern, *Can. J. Chem.*, 1959, **37**, 1903–1910.
- 18 H. S. Taylor, *Proc. R. Soc. London. Ser. A*, 1925, **108**, 105–111.
- 19 S. M. Oxford, J. D. Henao, J. H. Yang, M. C. Kung and H. H. Kung, *Appl. Catal. A Gen.*, 2008, **339**, 180–186.
- 20 M. M. Nigra, I. Arslan and A. Katz, *J. Catal.*, 2012, **295**, 115–121.
- 21 Y. Sun, B. Mayers, T. Herricks and Y. Xia, *Nano Lett.*, 2003, **3**, 955–960.
- 22 S. Hagen, P. Kate, M. V. Peters, S. Hecht, M. Wolf and P. Tegeder, *Appl. Phys. A Mater. Sci. Process.*, 2008, **93**, 253–260.
- 23 U. Jung, O. Filinova, S. Kuhn, D. Zargarani, C. Bornholdt, R. Herges and O. Magnussen, *Langmuir*, 2010, **26**, 13913–13923.
- 24 T. Solomun, K. Christmann and H. Baumgaertel, *J. Phys. Chem.*, 1989, **93**, 7199–7208.
- 25 E. R. McNellis, J. Meyer and K. Reuter, *Phys. Rev. B*, 2009, **80**, 205414.
- 26 M. E. Bartram and B. E. Koel, *Surf. Sci.*, 1989, **213**, 137–156.
- 27 W. Dozier, J. Drake and J. Klafter, *Phys. Rev. Lett.*, 1986, **56**, 197–200.
- 28 A. van Blaaderen and A. Vrij, *J. Colloid Interface Sci.*, 1993, **156**, 1–18.
- 29 J. Turkevich, P. C. Stevenson and J. Hillier, *Discuss. Faraday Soc.*, 1951, **11**, 55–75.
- 30 K. L. McGilvray, J. Granger, M. Correia, J. T. Banks and J. C. Scaiano, *Phys. Chem. Chem. Phys.*, 2011, **13**, 11914–11918.
- 31 C. Graf, D. L. J. Vossen, A. Imhof and A. Van Blaaderen, *Langmuir*, 2003, **19**, 6693–6700.
- 32 W. Stöber, A. Fink and E. Bohn, *J. Colloid Interface Sci.*, 1968, **26**, 62–69.